Semi-analytic approximations for production of atmospheric muons and neutrinos*

Thomas K. Gaisser
Bartol Research Institute, University of Delaware
Newark, DE 19716

February 1, 2008

Abstract

Simple approximations for fluxes of atmospheric muons and muon neutrinos are developed which display explicitly how the fluxes depend on primary cosmic ray energy and on features of pion production. For energies of approximately 10 GeV and above the results are sufficiently accurate to calculate response functions and to use for estimates of systematic uncertainties.

1 Introduction

There are several reasons for which it is useful to have simple approximations for production of muons and neutrinos by interactions of cosmic-ray nucleons in the atmosphere. First, the dependence on pion and kaon production, as well as the dependence on energy of the primary cosmic rays can be displayed explicitly. This is useful to make estimates of the systematic errors in the expected signals in muon and neutrino detectors that arise from uncertainties in the primary cosmic-ray spectrum and in meson production, which in general depend on energy.

The dependence of the signal in a particular detector on the primary energy spectrum is its response function. The classical use of response functions for muon telescopes [1] is to interpret measurements of solar modulation of muons as a function of muon energy and geomagnetic latitude [2]. In addition, response functions are useful for planning and optimizing Monte Carlo simulations of detectors because they display explicitly the relative portion of the signal that comes from each part of the primary spectrum.

For power-law spectra the analytic approximations for fluxes of muons and neutrinos are well-known [3, 4, 5]. In this paper we develop approximations which also display the dependence on primary energy. Such approximations allow semi-analytic evaluation of response functions. They can also be used to estimate the muon-induced signal produced by a fluence of protons with an arbitrary energy spectrum and time profile, such as might be associated with a strong solar event.

*This research is supported in part by the US Department of Energy grant DE-FG02 91ER 40626.

The approximate results here are valid for muons and muon-neutrinos at relatively high energy, of order ten GeV and above. This includes the interesting cases of underground measurements of atmospheric muons and of upward energetic muons induced by atmospheric neutrinos. The same results can, of course, be obtained with greater precision and for low energies, including electron neutrinos, by Monte Carlo simulations or by more complicated numerical calculations. The analytic approximations are nevertheless useful for the insight they provide and for the diagnostic purposes mentioned above.

2 Derivation of analytic approximations

The differential production spectra of muons and neutrinos of energy E from decay of pions in atmospheric cosmic ray cascades are given by

$$\frac{dN}{dE\, dE_\pi dE_N dX} = \frac{S(E,E_\pi)}{(1-r_\pi)E_\pi}\frac{1}{d_\pi}\int_0^X \frac{dX'}{\lambda_N}\, P_\pi(E_\pi,X,X') \times\frac{1}{E_\pi}F_{N\pi}(E_\pi,E_N)\, e^{-X'/\Lambda_N}\,\phi(E_N), \quad (1)$$

where $P_\pi(E_\pi,X,X')$ is the probability that a charged pion produced at slant depth X' (g/cm^2) survives to depth $X\,(>\,X')$. For muons the kinematic factor, $S(E,E_\pi)$, has the form

$$S_\mu(E_{\mu,0},E_\pi) \,=\, \Theta(E_\pi - E_{\mu,0})\,\Theta(\frac{E_{\mu,0}}{r_\pi} - E_\pi), \quad (2)$$

while for muon neutrinos it is

$$S_{\nu_\mu}(E_\nu,E_\pi) \,=\, \Theta(E_\pi - \frac{E_\nu}{(1-r_\pi)}), \quad (3)$$

where $r_\pi \,=\, \frac{m_\mu^2}{m_\pi^2}$. Here Θ is the Heaviside step function, and the subscript $_0$ in Eq. 2 indicates muon energy at production (see Appendix).

The contribution from kaon-decay has the same form as Eq. 1 with appropriate changes in kinematic factors and an overall factor for the branching ratio of $B_{K\to\mu\nu} \,=\, 0.635$. The various parameters relevant for $N \to [K,\pi] \to \mu\nu_\mu$ are summarized in Table 1. The differences between the decay parameters for kaons and pions and between the mass ratios, r_π and r_K are responsible for the striking difference between the importance of kaons for neutrinos as compared to muons. In particular, kaons become the dominant source of atmospheric neutrinos for E_ν larger than ~ 100 GeV even though more pions than kaons are produced.

The integral in Eq. 1 is over atmospheric depth X' measured in g/cm^2 along the trajectory of the incident particle at zenith angle θ. The nucleon interaction length is λ_N. The factor $\exp\{-X'/\Lambda_N\}\,\phi(E_N)$ is the flux of nucleons of energy E_N at slant depth X', where Λ_N is the nucleon attenuation length in the atmosphere and $\phi(E_N)$ is the primary spectrum of nucleons per GeV/nucleon. The superposition approximation [6] is used for nucleons bound in nuclei.

The normalized inclusive cross section for N + air $\to \pi^\pm + X$ is

$$F_{N\pi}(E_\pi,E_N) \,=\, \frac{E_\pi}{\sigma_N}\,\frac{d\sigma(E_\pi,E_N)}{dE_\pi} \approx c_+(1-x)^{p_+} \,+\, c_-(1-x)^{p_-}, \quad (4)$$

Table 1: Parameters for atmospheric $\mu^+ + \mu^-$ and $\nu_\mu + \bar{\nu}_\mu$

Mass-square ratios:	r_π	r_K		
	0.573	.046		
Characteristic E_{decay}:	ϵ_π	ϵ_K	ϵ_μ	
	115 GeV	850 GeV	1 GeV	
Attenuation lengths:	Λ_π	Λ_K	Λ_N	λ_N
	160 g/cm^2	180 g/cm^2	120 g/cm^2	86 g/cm^2

Table 2: Parameters for kaon and pion production

	c_+	p_+	Z_+	c_-	p_-	Z_-
charged pions	0.92	4.1	0.047	0.81	4.8	0.034
charged kaons	0.037	0.87	0.0089	0.045	3.5	0.0028

where $x = x_\pi = E_\pi/E_N$. The parameters of this scaling approximation are fixed by comparison to accelerator data in the sub-TeV range [4], and the adequacy of the simple approximation is verified later by comparison of the calculated neutrino flux to the result of a complete Monte Carlo calculation. A more complicated or precise expression could be used for the inclusive cross section if desired. The expressions for kaons have the same form, and the numerical values used in this paper are given in Table 2.

The survival probability in Eq. 1 is a product of survival against decay and survival against interaction.

$$P_\pi(E_\pi, X, X') \;=\; \left(\frac{X'}{X}\right)^{\epsilon_\pi/E_\pi \cos\theta} \exp\{-(X - X')/\Lambda_\pi\}. \tag{5}$$

Use of the pion attenuation length, Λ_π, rather than the pion interaction length, $\lambda_\pi < \Lambda_\pi$, in the interaction factor of Eq. 5 accounts approximately for the regeneration of charged pions when pions interact in the atmosphere. The first factor in Eq. 5 is the probability for survival against decay, and the explicit form used here is valid in the approximation of an exponential atmosphere with scale height h_0 and decay constant $\epsilon_\pi = m_\pi c^2 h_0/c\tau_\pi$.

Finally, $1/d_\pi = \epsilon_\pi/(E_\pi X \cos\theta)$ is the differential pion decay probability (per g/cm^2) in an exponential atmosphere. The simple angular dependence displayed here is valid when the curvature of the Earth can be neglected ($\theta \leq 60°$). For large angle the analysis is more complicated, but one approach is to use the same form with $\cos\theta$ replaced by an effective value that depends on θ [7].

The next step is to carry out the integral over the production depth, X', in Eq. 1. This is done by expanding the exponential of X' and expressing the result as a series of the form

$$\frac{1}{d_\pi}\int_0^X P_\pi(E_\pi, X, X')\, e^{-X'/\Lambda_N}\, \frac{dX'}{\lambda_N} \;=\; \frac{e^{-X/\Lambda_\pi}}{\lambda_N} \sum_{n=1}^{\infty} \left(\frac{X}{\Lambda_\pi}(-a_\pi)\right)^{n-1} \frac{1}{n!(1 + nE_\pi \cos\theta/\epsilon_\pi)}, \tag{6}$$

where $a_\pi = \Lambda_\pi/\Lambda_N - 1 \approx 0.33$. Substituting this expression into Eq. 1 we can now integrate over all depths X of pion decay. The upper limit of this integral can safely be extended to infinity since most production of secondaries occurs well above the ground.

The result for $\nu_\mu + \bar{\nu}_\mu$ is

$$\frac{dN}{dE_\nu\, dE_\pi dE_N} \;=\; \frac{S_\nu(E_\nu, E_\pi)}{(1-r_\pi)E_\pi}\,\frac{1}{E_\pi} F_{N\pi}(E_\pi, E_N)\, G_\pi(E_\pi, \theta)\, \phi(E_N). \tag{7}$$

The physics of cascade propagation is included in Eq. 7 by the factor

$$G_\pi(E_\pi, \theta) \;=\; \frac{\Lambda_\pi}{\lambda_N} \sum_{n=1}^{\infty} \left\{ \frac{(-a_\pi)^{n-1}}{1 + n\, E_\pi\, \cos\theta/\epsilon_\pi} \right\}. \tag{8}$$

The contribution from kaons has the same form with $a_K = \Lambda_K/\Lambda_N - 1 \approx 0.5$.

The dependence on the inclusive cross sections for pion (and kaon) production by nucleons can be displayed immediately in the approximation of a power-law primary spectrum by changing variables from $\{E_\nu, E_\pi, E_N\}$ to $\{E_\nu, x_\pi, z = x_\pi E_N\}$ and integrating over z to obtain

$$\frac{dN}{dE_\nu dx_\pi} \;=\; (x_\pi)^{\gamma-1}\, \frac{F_{N\pi}(x_\pi)}{1-r_\pi} \int_{E_\nu/(1-r_\pi)}^{\infty} \frac{dz}{z}\, G_\pi(z, \theta)\, \phi(z), \tag{9}$$

where γ is the integral spectral index. The dependence on pion production by nucleons appears here as an explicit proportionality factor, the integral of which is the Z-factor,

$$Z_{N\to\pi} \;=\; \int_0^1 dx\, (x)^{\gamma-1}\, F_{N\to\pi}(x), \text{ etc..} \tag{10}$$

The dependence on nucleon production by nucleons and on pion [kaon] production by pions [kaons] does not appear explicitly in Eq. 9. Dependence on these processes is contained in the attenuation lengths, Λ_N and Λ_π [Λ_K]. which appear respectively in Eq. 1 and in the expression for G_π [G_K] as defined in Eq. 8. The attenuation lengths are related to the respective interaction lengths and inclusive cross sections by $\Lambda_i = \lambda_i/(1 - Z_{i\to i})$, where i stands for nucleon (N = p or n), charged pion or charged kaon. Note from Eq. 8 that Λ_π cancels out of the expression when $E_\pi/\epsilon_\pi \ll 1$, reflecting the fact that low energy pions [kaons] usually decay before they interact. The small cross processes $K^\pm \leftrightarrow \pi^\pm$, as well as neutral kaons, are neglected as sources of ν and μ in these approximations.

3 Response Functions and Fluxes

To obtain the response function, the integral over pion energy is carried out in Eq. 7 making use of the scaling approximation of Eq. 4. The flux of $\nu_\mu + \bar{\nu}_\mu$ with zenith angle θ from decay of $\pi^+ + \pi^-$ is given by

$$E_N\, \frac{dN_\nu}{dE_\nu dE_N}\bigg|_\pi \;=\; \frac{\phi(E_N)}{1-r_\pi} \int_{x_\nu/(1-r_\pi)}^1 dx\, G_\pi(E_N x, \theta)\, \frac{F_\pi(x)}{x^2}, \tag{11}$$

where $x_\nu = E_\nu/E_N$. The contribution from kaons has the same form.

In the absence of muon decay and energy loss, the expression for the response function for muons would be identical to that for neutrinos except that the limits of the integration in Eq. 11 are changed to those appropriate for muons (Eq. 2 instead of 3). They are

$$x_{min} \;=\; \frac{E_{\mu,0}}{E_N} \;\text{ and } x_{max} \;=\; \min\left[1,\, \frac{x_{min}}{r_\pi}\right].$$

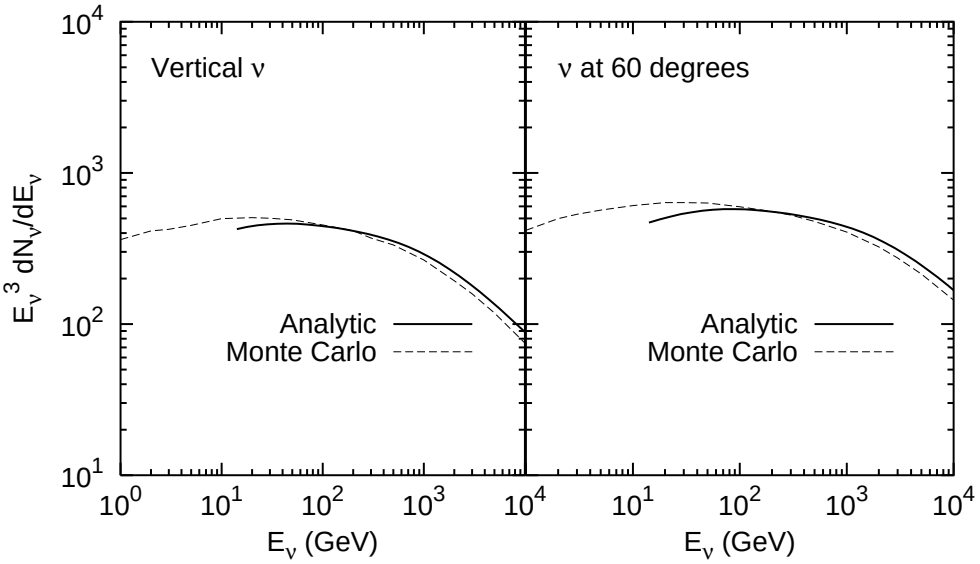

Figure 1: Comparison of the analytic approximation (solid) for the flux of $\nu_\mu + \bar{\nu}_\mu$ with the result of the full Monte Carlo (dashed) [8].

In the Appendix an approximate treatment is given for the effects of muon decay and energy loss that can be used for $E_\mu \sim 10$ GeV and higher. In this approximation,

$$E_{\mu,0} \approx \left(E_\mu + \frac{2\,\mathrm{GeV}}{\cos\theta} \right),$$

and

$$E_N \left. \frac{dN_\mu}{dE_\mu dE_N} \right|_\pi = \frac{\phi(E_N)}{1 - r_\pi} A(E_\mu) \int_{x_{min}}^{x_{max}} dx\, G_{\pi,\mu}(E_N x, \theta) \frac{F_\pi(x)}{x^2}, \tag{12}$$

with

$$G_{\pi,\mu}(E_N x, \theta) = \frac{\Lambda_\pi}{\lambda_N} \sum_{n=1}^{\infty} C_n(E_\mu) \left\{ \frac{(-a_\pi)^{n-1}}{1 + n E_N\, x\, |\cos\theta| / \epsilon_\pi} \right\}. \tag{13}$$

The functions $A(E_\mu)$ and $C_n(E_\mu)$ are defined in the Appendix.

The differential fluxes are then obtained in both cases by summing the contributions from pions and kaons and integrating over E_N. The analytic approximations for the fluxes of $\nu_\mu + \bar{\nu}_\mu$ and $\mu^+ + \mu^-$ are compared with the results of the full Monte Carlo calculation [8] at two angles in Figs 1 and 2. The values of parameters that have been used in the analytic approximations are listed in Tables 1 and 2. They correspond most closely to the hadroproduction model of Ref. [8] for interaction energies around 100 GeV. The approximation falls below the neutrino flux at low energy primarily because the contribution from muon decay is not included in the approximation. At high energy the approximation is 10-15% higher than the Monte Carlo, because the simple, energy-independent forms for kaon production used here are not identical to the actual representation in the Monte Carlo. The analytic approximations could be tuned to give a better representation of this [8] or any other interaction model, but doing so is not the object of this paper. The approximate results

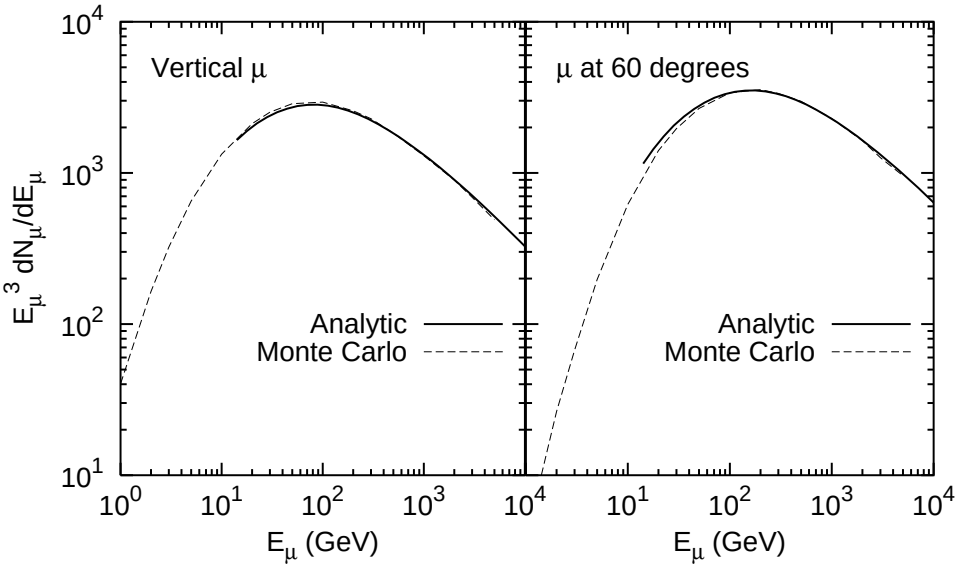

Figure 2: Comparison of the analytic approximation (solid) for the flux of $\mu^+ + \mu^-$ with the result of the full Monte Carlo (dashed) [8].

are sufficiently accurate that the analytic calculation may be used for diagnostic purposes above 10 GeV where the contributions from muon decay are unimportant. These include propagation of errors, calculation of response functions and evaluation of the phase space regions that are most important for the determining the fluxes of neutrinos and muons.

In Fig. 3 I show the fractions of $\nu_\mu + \bar{\nu}_\mu$ from $\pi^\pm$ and from $K^\pm$ to demonstrate the importance of kaon production. Note that over the entire energy region, approximately 70-75% of ϕ_ν comes from free protons (most of the rest is from nucleons in primary helium) [9]. Thus, any uncertainty from the approximate, superposition model treatment [6] of bound nucleons will be small.

Having established that the method is adequate, the next step is to calculate the response functions for a range of energies. This is illustrated in Fig. 4 for muons and neutrinos. Note that the neutrino response is shifted to higher primary energy than the response for muons. In addition, it is slower to reach an asymptotic form. These features are consequences of the kinematics of $\pi \to \mu\nu_\mu$ as compared to $K \to \mu\nu_\mu$ coupled with the greater relative importance of kaons for neutrinos at high energy. Pions must have more than twice the energy of daughter ν_μ, while $E_\pi \geq E_{\mu,0}$ (compare Eqs.2,3). This shifts the ν_μ response to higher energy when the pion chain is dominant. At higher energy, where kaons dominate the production of ν_μ the response shifts to lower energy.

4 Estimates of Uncertainties

To illustrate how the formalism presented here can be used to estimate uncertainties in the calculated result, we consider the example of vertically upward, neutrino-induced, through-going muons at Super-Kamiokande [10]. The distribution of neutrino energies

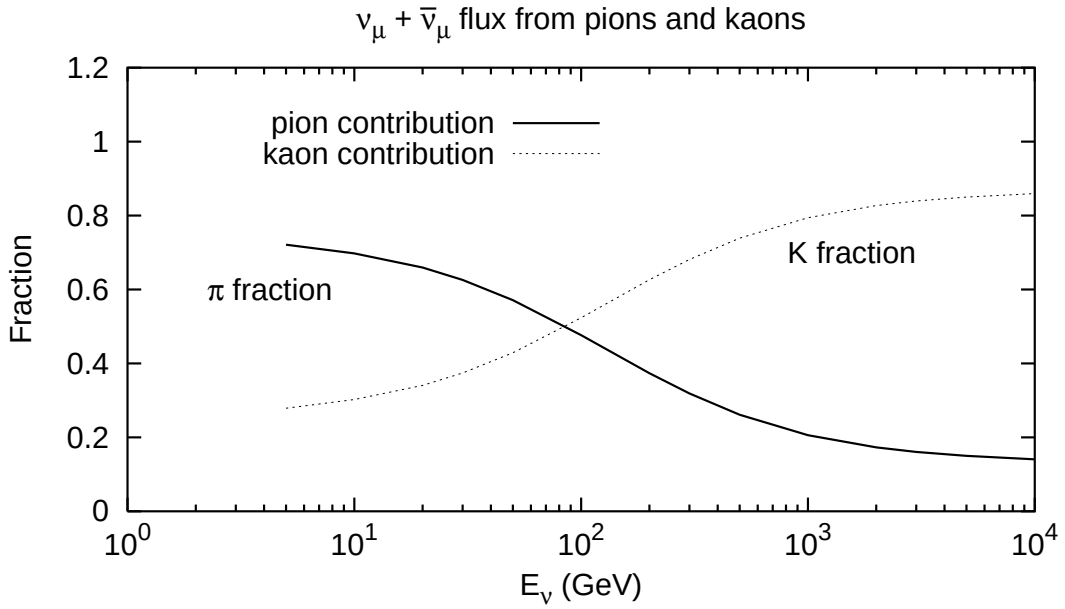

Figure 3: Plot showing fractional contribution of pions and kaons to the flux of $\nu_\mu + \bar{\nu}_\mu$.

that produce this signal (in the absence of oscillations) is shown as the light solid line [11] in Fig. 5. The heavy line shows the corresponding distribution of parent nucleon energies. This distribution should be used to weight the uncertainties in the input in a convolution over primary energy. A similar analysis can be made for neutrino-induced muons that stop inside the detector.

There are two main sources of uncertainties in calculations of fluxes of muons and neutrinos with energies in the multi-GeV range and above. We deal first with those arising from uncertainties in the primary spectrum and then with those from uncertainties in treatment of pion and kaon production.

4.1 Primary spectrum

Since approximately 75% of high energy atmospheric neutrinos are produced by incident protons, I concentrate on that component of the cosmic-ray spectrum for the analysis of uncertainties. A summary of data is shown in Fig. 6. The solid line is the proton spectrum used in Ref. [8], which I take as the reference spectrum. The resulting uncertainty in the flux of atmospheric neutrinos that is relevant for the Super-K example will be a convolution of the uncertainties in the data of Fig. 6 with the response function shown as the heavy solid line in Fig. 5.

It is natural to divide the discussion into three energy regions:

4.1.1 Up to ~ 100 GeV

Primaries with energies below 100 GeV are the most precisely measured. They make the major contribution to contained neutrino events, but only a small contribution to

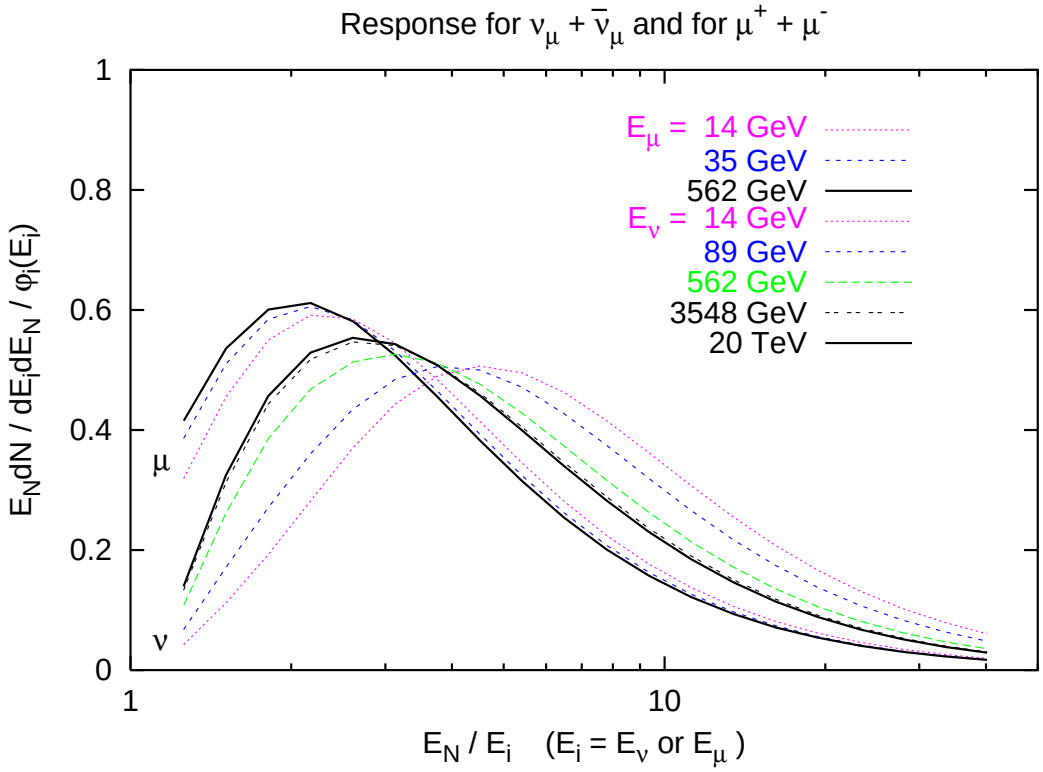

Figure 4: The distributions of primary energy per nucleon (E_N) that give rise to vertical $\nu_\mu + \bar{\nu}_\mu$ of energy E_ν (right-hand set of curves) and to $\mu^+ + \mu^-$. Each curve is normalized to unity. For each set the lowest energy is the rightmost curve. The response is approximately energy-independent for $E_\nu > 3$ TeV and for $E_\mu > 30$ GeV when expressed in terms of E/E_N.

neutrino-induced upward muons. While they do not cover the full range of interest they can be used to renormalize the single measurement [19] that spans the important energy range up to $\sim$ 1 TeV. Several measurements have been made in the past decade with balloon-borne magnetic spectrometers capable of making relatively precise momentum measurements for well-identified protons and nuclei. Since the LEAP experiment [12], five other experiments [13, 14, 15, 16, 17] confirm a significantly lower normalization than the earlier standard reference [18]. Particularly noteworthy are the BESS98 [17] and the AMS [15] measurements, which agree with each other to within 5% over two decades in energy. These data have been used as the basis of a new fit [9] as shown in Fig. 6. The systematic uncertainty in the primary spectrum below 100 GeV is estimated in Ref. [9] as $< \pm 5\%$.

4.1.2 Up to $\sim$ 1 TeV

The energy region from 0.1 to 2 TeV, explored by the large balloon-borne tracking calorimeter of Ryan *et al.* [19], is of great importance for ν_μ-induced upward muons. We renor-

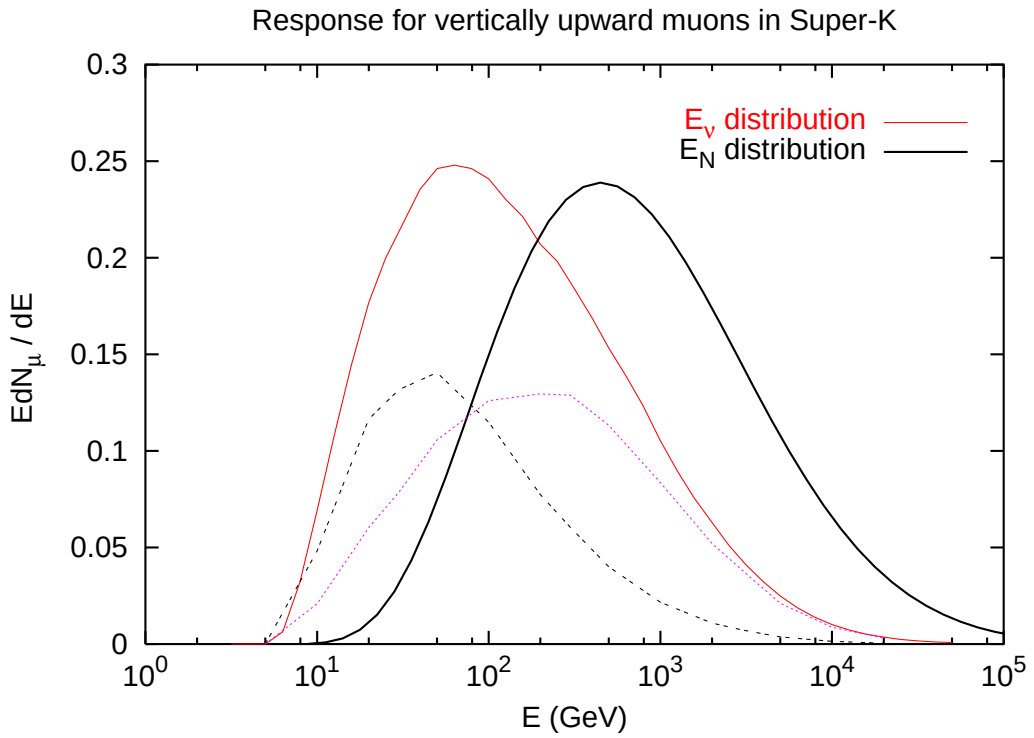

Figure 5: Distribution of neutrino energy (light solid) and primary nucleon energy (heavy solid) that produce the through-going, vertically upward signal at Super-Kamiokande. Each curve is normalized to unity. The contributions of pions (double dash) and of kaons (dotted) are shown as a function of neutrino energy.

malize the Ryan *et al.* data downward by 25 % to agree with the magnetic spectrometer data below 100 GeV [9]. Note that the normalization can reflect a smaller shift in energy calibration because of the steep spectrum [9]. This renormalization brings the measurement of Ryan *et al.* into agreement with the reference spectrum. The remaining overall uncertainty in this energy region is $\sim \pm 10\%$.

4.1.3 The multi-TeV region

Most of the data in this energy range comes from balloon flights of emulsion chambers, [20, 21, 23] which measure only the electromagnetic component of the energy deposited by the interacting proton in the chamber. This is subject to large fluctuations superimposed on the uncertainty in the underlying inelasticity distribution of protons when they interact in the emulsion chamber. There is also one measurement in this energy region made with a tracking calorimeter carried on flights of the SOKOL satellite [22].

The uncertainties in these measurements are at the level of $\pm 25\%$. In addition, there is an indication that the flux falls below the reference spectrum above ~ 20 TeV by up to a factor of 2. However, the contribution from protons with $E_N > 20$ TeV to the energy range responsible for ν_μ-induced upward muons is small.

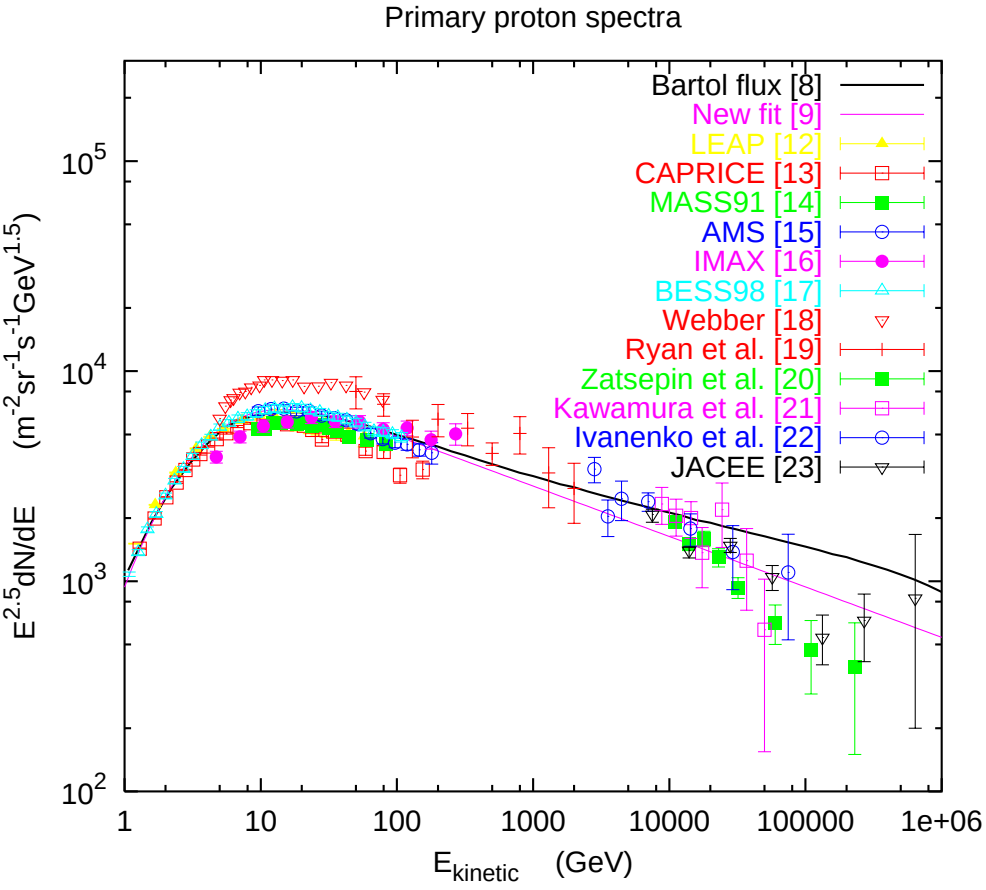

Figure 6: Summary of measurements of the spectrum of cosmic-ray protons. Data are from [12, 13, 14, 15, 16, 17, 18, 19, 20, 21, 22, 23].

4.2 Dependence on pion and kaon production

The dependence on the phase space for pion and kaon production is displayed in Eq. 9, which is illustrated for several values of neutrino energy in Fig. 7. The figure illustrates the growing relative importance of kaons. It also illustrates the importance of the extreme forward fragmentation region for the contribution of kaons, reflecting the leading $p \rightarrow \Lambda + K^+$ process. The shapes are scale invariant in the approximations used here, and they indicate the regions of phase space that are important for production of atmospheric neutrinos.

A global estimate of the uncertainty due to pion and kaon production is obtained, as in Ref. [8], by estimating the uncertainty in the Z-factors for pions and kaons and weighting them according to Figs. 3 and 5.

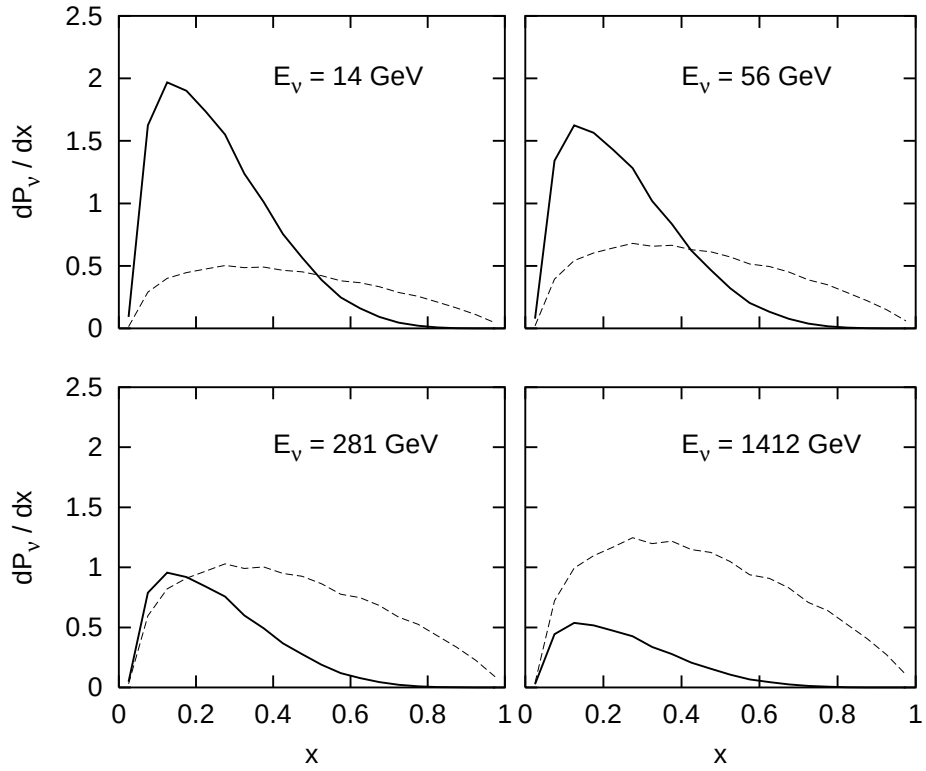

Figure 7: Phase space distributions for parents of $\nu_\mu + \bar{\nu}_\mu$ from decay of $\pi^\pm$ and $K^\pm$ at four values of E_ν. Solid lines are for pions and dashed for kaons. The curves are normalized to unity at each energy for the sum of $\pi \to \nu$ and $K \to \nu$. from pions and from kaons.

4.3 Illustration

To obtain a simple estimate of the overall uncertainty in the signal of upward-moving muons due to the uncertainty in the spectrum of atmospheric neutrinos, we combine the estimates of several sources of uncertainty as if they were independent, statistical uncertainties. For upward, through-going muons in Super-Kamiokande, as shown in Fig. 5, the three energy regions of the primary spectrum, < 0.1 TeV, $0.1 < E_N < 1$ TeV and > 1 TeV contribute respectively fractions of 0.2, 0.4 and 0.4 to the signal. Weighting and adding the corresponding three uncertainties ($\pm.05$, $\pm.10$, $\pm.25$) in quadrature gives an overall uncertainty of $\pm 11\%$ due to the primary spectrum. Uncertainties in $Z_{N\pi}$ and Z_{NK} are estimated in Ref. [8] as $\pm 12\%$ and $\pm 17\%$ respectively. Roughly equal fractions of the signal are from pions and kaons, so the combined uncertainty from the interaction model is $\sim \pm 10\%$ giving an overall estimated uncertainty of $\pm 15\%$.

For upward, stopping muons in Super-K, the corresponding analysis shows that essentially all the signal comes from primaries with $E < 1$ TeV/nucleon, of which $\sim 60\%$ are in the well-measured region between 10 and 100 GeV. Thus the weighted uncertainty due to uncertainty in the primary spectrum is estimated as $\pm 5\%$. For this lower energy sam-

ple, approximately two-thirds are from decay of pions, so the weighted uncertainty from hadronic interactions is also somewhat smaller than for through-going muons, $\pm 10\%$, giving a combined uncertainty of $\pm 11\%$.

Combining these two numbers results in an estimate of $\pm 19\%$ for the uncertainty in the calculated ratio of stopping to through-going neutrino-induced, upward muons in Super-K expected in the absence of oscillations.

5 Summary

The main results of the paper are contained in Eq. 9 and in Eqs. 11 and 12 [and the corresponding expressions for kaons]. Eq. 9 displays explicitly how the flux depends on the phase space for pion [kaon] production. One can see from the corresponding plots which regions of phase space need to be measured in experiments such as HARP [24], in order to improve the input to calculations of atmospheric neutrinos.

Eqs. 11 and 12 show respectively the response functions for ν_μ and for muons. These can be convolved with the response of an underground detector to neutrinos or muons to show how the signal depends on the primary spectrum. The response functions in Fig. 4 can also be used as an aid in planning a Monte Carlo calculation of atmospheric muon or neutrino fluxes and their signals in a particular detector. By knowing the distribution of primary energies that contribute to the neutrino (or muon) flux at $E_{\nu(\mu)}$, one can determine in advance the range and distribution of primary energies needed to obtain a result with sufficient statistical accuracy.

Since the formulas 11 and 12 display the dependence on primary energy explicitly, they can also be used to estimate the signal from a primary spectrum of arbitrary shape and evolution, such as might be associated with a violent solar flare. Applications to calculation of neutrino fluxes in astrophysical beam dumps (with appropriately modified cascade propagation factors, $G_{\pi,\mu}$) are also possible.

In §4 we gave an example of the use of the semi-analytic approach in estimating "theoretical" uncertainties in an expected neutrino-induced signal. A complementary approach is simply to compare different, independent calculations of the spectrum of atmospheric neutrinos. Fig. 8 shows a comparison of four calculations. The calculations of Ref. [8] and [25] are one-dimensional Monte Carlo calculations. The calculation of Ref. [5] is an analytic calculation assuming a pure power-law primary spectrum of nucleons and scaling for the inclusive cross sections. These three calculations are within a range of $\approx 10\%$ of each other over the relevant range of energies. Several earlier calculations are compared in Fig. 7 of Ref. [8] and are also within this range. The three-dimensional calculation of Battistoni *et al.* [26] is shown by the points in the figure. (Because of the complexity of the 3-D calculation, statistics in the near vertical bin are limited at present, especially so at the high-energy end [27].) The calculation of Ref. [26] assumed the same primary spectrum as used in Ref. [8]. In addition, the energy range here is well into the region for which three-dimensional effects can be neglected. The differences are therefore presumed to be a result of differences in the representation of pion and kaon production. The authors of the calculations shown in Fig. 8 are in the process of comparing hadronic interaction models with the goal of minimizing this source of uncertainty in the calculations of atmospheric muons and neutrinos.

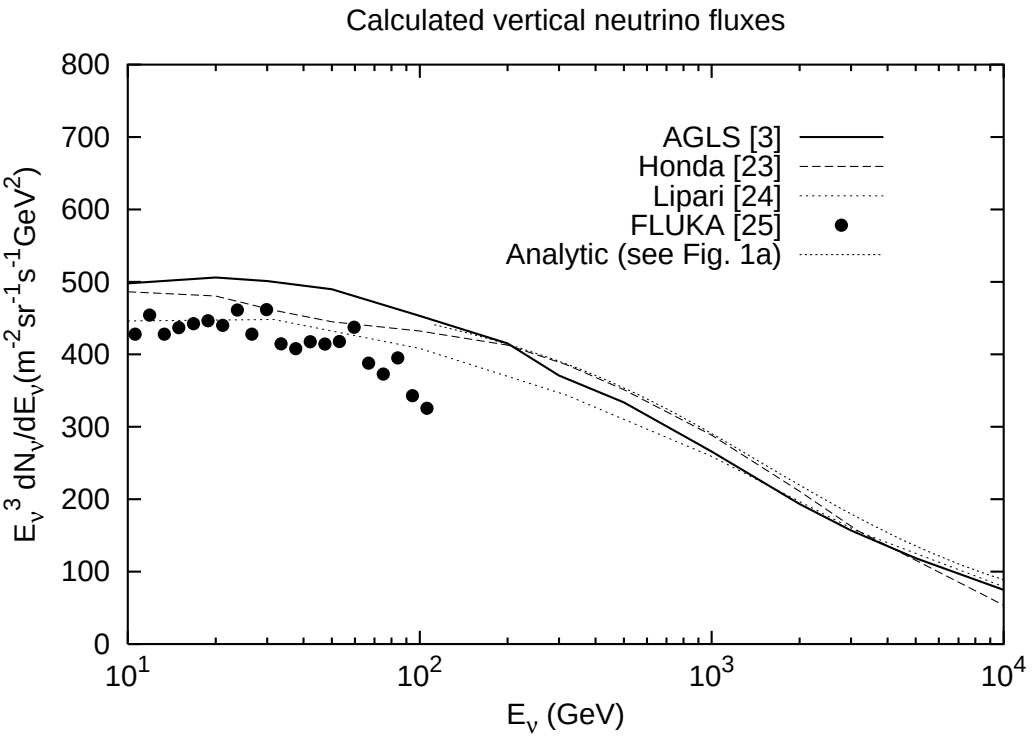

Figure 8: Comparison of three calculations of the vertical flux of atmospheric neutrinos $(\nu_\mu + \bar{\nu}_\mu)$ [8, 25, 5].

6 Appendix: Approximate treatment of muon decay and energy loss

For muons, which lose energy and which may decay in the atmosphere before reaching the ground, we must first multiply by the muon survival probability and take account of muon energy loss between production at depth X and the ground at vertical atmospheric depth $X_0 \approx 1030 g/cm^2$. This is done by multiplying Eq. 1 by the muon survival probability before integrating over the depth, X, of pion (or kaon) decay. The muon survival probability given by Lipari [5] can be rewritten in the form

$$P_\mu(E_\mu, X, X_0) \;=\; \left(\frac{X \cos\theta}{X_0} \frac{E_\mu}{E_\mu + \alpha(X_0/\cos\theta - X)} \right)^{\epsilon_\mu/(E_\mu \cos\theta + \alpha X_0)} , \qquad (14)$$

Here E_μ is the muon energy at the ground, whereas its energy at production in Eq. 2 is $E_{\mu,0} = E_\mu + \alpha(X_0/\cos\theta \; - \; X)$.

To simplify the integration, I make the approximation of replacing X in the expression for $E_{\mu,0}$ and in Eq. 14 by $\Lambda_N \approx 120$ g/cm^2, which is its mean value at low energy ($E_\mu < E_\pi \ll \epsilon_\pi \approx 115$ GeV). Ionization energy loss is characterized by $\alpha \approx 2$ MeV/g/cm^2, so $E_{\mu,0} \approx E_\mu + 2$ GeV$/cos\theta$, and the approximate forms will be valid for $E_\mu \gg 2/\cos\theta$ GeV, in practice, for $E_\mu > 10$ GeV for the applications of this paper.

For high energy, ionization energy loss is negligible, but radiative losses due to pair production, bremsstrahlung, and hadronic interactions of muons begin to become important. However, the radiation lengths are sufficiently large that the probability of significant radiative energy losses in the atmosphere is small, and they have been neglected here.

With these approximations, we can now follow the same steps used to obtain Eq. 7. The result is

$$\begin{aligned} \frac{dN}{dE_\mu\, dE_\pi dE_N} &= \frac{S_\mu(E_{\mu,0}, E_\pi)}{(1-r_\pi)E_\pi} \frac{1}{E_\pi} F_{N\pi}(E_\pi, E_N) \\ &\times \frac{\Lambda_\pi}{\lambda_N}\, A(E_\mu) \sum_{n=1}^{\infty} C_n(E_\mu)\, \frac{(-a_\pi)^{n-1}}{1 + nE_\pi \cos\theta/\epsilon_\pi}\, \phi(E_N). \end{aligned} \tag{15}$$

Here

$$A(E_\mu) = \left(\frac{\Lambda_\pi \cos\theta}{X_0} \frac{1}{1 + 2/E_\mu \cos\theta} \right)^{\epsilon_\mu/((E_\mu \cos\theta + 2)}$$

and

$$C_n = C_{n-1} \times \left(1 + \frac{\epsilon_\mu}{(n-1)(E_\mu \cos\theta + 2)} \right)$$

with

$$C_1 = \Gamma \left(1 + \frac{\epsilon_\mu}{(E_\mu \cos\theta + 2)} \right)$$

References

[1] T.K. Gaisser, J. Geophys. Res. 79 (1974) 2281.

[2] Martin A. Pomerantz, *Cosmic Rays* (Van Nostrand Reinhold Company, New York, 1971) pp. 86-69.

[3] W.R. Frazer *et al.*, Phys. Rev. D5 (1972) 1653. see also Yash Pal & Bernard Peters Mat. Fys. Medd. Dan. Vid. Selsk. 33(15) (1964) 1.

[4] *Cosmic Rays and Particle Physics*, T.K. Gaisser, Cambridge University Press (1992).

[5] Paolo Lipari, Astroparticle Physics 1 (1993) 195.

[6] J. Engel *et al.*, Phys. Rev. D46 (1992) 5013.

[7] T.K. Gaisser & Todor Stanev, Phys. Rev. D57 (1998) 1977.

[8] Vivek Agrawal, T.K. Gaisser, Paolo Lipari & Todor Stanev, Phys. Rev. D53 (1996) 1314.

[9] T.K. Gaisser, M. Honda, Paolo Lipari & Todor Stanev, in preparation.

[10] Y. Fukuda *et al.*, Phys. Rev. Letters 82 (1999) 2644.

[11] R. Engel, T.K. Gaisser & Todor Stanev, Phys. Letters B 472 (2000) 113.

[12] E.S. Seo *et al.*, Ap.J. 378 (1991) 763.

[13] M. Boezio *et al.* Ap.J. 518 (1999) 457.

[14] R. Bellotti *et al.*, Phys. Rev. D60 (1999) 052002.

[15] J. Alcaraz *et al.*, Physics Letters B 490 (2000) 27.

[16] W. Menn, *et al.*, Ap.J. 533 (2000) 281.

[17] T. Sanuki *et al.*, astro/ph-0002481

[18] W.R. Webber *et al.* Proc. 20th Int. Cosmic Ray Conf. (Moscow) vol. 1 (1987) 325.

[19] M.J. Ryan, J.F. Ormes & V.K. Balasubrahmanyan, Phys. Rev. Letters 28 (1972) 985 & E1497. (Calgary) vol. 2 (1993) 17.

[20] V.I. Zatsepin *et al.*, Proc. 23rd Int. Cosmic Ray Conf. (Calgary) vol. 2 (1993) p. 13.

[21] Y. Kawamura *et al.*, Phys. Rev. D40 (1989) 729.

[22] I.P. Ivanenko *et al.*, Proc. 23rd Int. Cosmic Ray Conf.

[23] K. Asakimori *et al.*, Ap. J. 502 (1998) 278.

[24] The HARP Experiment, http://harp.web.cern.ch/harp/.

[25] M. Honda *et al.*, Phys. Rev. D52 (1995) 4985.

[26] G. Battistoni *et al.* Astroparticle Physics 12 (2000) 315.

[27] Neutrino fluxes from the 3-D calculation are at http://www.mi.infn.it∼battist/neutrino.html.